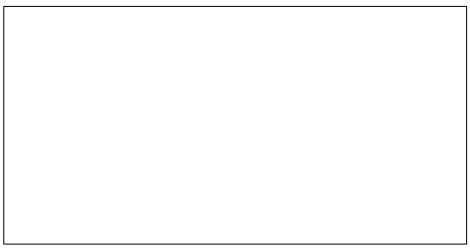

Available online at www.sciencedirect.com

ScienceDirect

Procedia Computer Science 60 (2015) 1613 – 1621

Procedia Computer Science

19th International Conference on Knowledge Based and Intelligent Information and Engineering Systems

An Evaluation of Image Enhancement Techniques for Nailfold Capillary Skeletonisation

Niraj P. Doshi[a], Gerald Schaefer[b], Shao Ying Zhu[c]

[a] *dMacVis Research Lab, India*
[b] *Department of Computer Science, Loughborough University, U.K.*
[c] *Department of Computing and Mathematics, University of Derby, U.K*

Abstract

Nailfold capillaroscopy (NC) is a routine technique used to assess the characteristics and morphology of nailfold capillaries. Observation of micro-blood vessels in the nailfold is important for diagnosing diseases that lead to morphological changes of capillaries such as scleroderma, Raynaud's phenomenon and other connective tissue diseases. In order to support a computer-aided diagnosis approach to analysing NC images, several approaches have been proposed in the literature aiming to extract capillaries. In general, such capillary skeletonisation algorithms involve an image pre-processing step, followed by binarisation and finally extraction and definition of the capillary skeletons. Since image denoising and enhancement in the pre-processing step can have a major impact on the subsequent analysis, in this paper, we evaluate the performance of five enhancement techniques for the purpose for nailfold capillary skeletonisation. In particular, we investigate the α-trimmed filter, bilateral filter, bilateral enhancer, anisotropic diffusion filter and non-local means and integrate them with three capillary extraction algorithms from the literature. We report visual and quantitative performance on a set of diverse NC images. The obtained results indicate that a relatively simple α-trimmed filter, combined with a skeletonisation algorithm incorporating a difference-of-Gaussian approach to address non-uniform lighting and an iterative rule-based skeletonisation procedure, leads to the best results when comparing the obtained skeletonisations to a manually obtained ground truth.

Peer-review under responsibility of KES International

Keywords: Medical imaging; nailfold capillaroscopy; image enhancement; pre-processing; skeletonisation;

1. Introduction

Various diseases including systemic sclerosis[1], Raynaud's phenomenon[2], as well as other connective tissue diseases such as dermatomyositis, antiphospholipid syndrome[3], and Sjögren's syndrome[4] lead to morphological changes of blood capillaries and can hence be diagnosed using nailfold capillaroscopy (NC), a passive, inexpensive in-vivo technique to observe micro-blood vessel characteristics in the nailfold region of fingers.

Diagnosis is typically performed by counting and/or identifying particular capillary types and other features such as enlarged or giant capillaries, haemorrhages, loss of capillaries, disorganisation of the vascular array, and ramified/bushy capillaries[5]. Specific NC patterns based on these features – *early*, *active* and *late* patterns – are routinely used to characterise NC images and to identify scleroderma and other diseases[6].

Peer-review under responsibility of KES International
doi:10.1016/j.procs.2015.08.271

Inspection of NC images is conventionally conducted manually and based on measurement of morphological parameters and the consultant's expertise. Thus, it constitutes a time consuming and specialised task which motivates the use of a computer-aided diagnosis (CAD) approach. However, relatively little work has been reported aimed at CAD from NC images. In[7], a panoramic mosaic image is generated from several video frames, which in turn helps to extract capillary shapes. In[8], the authors focussed on semi-automatic extraction of morphological features using various algorithms for vessel tracking, thickness analysis, and curvature analysis. Capillary condition analysis through classification is proposed in[9] and[10], while in[11] a set of rules is established to determine the progression of disease. While classification into NC patterns typically involves the extraction and measurement of single capillaries, in[12] a holistic approach is presented that performs identification of scleroderma patterns based on global texture features.

NC CAD techniques are thus typically based on capillary extraction from the NC image before performing any measurement analysis. Consequently, reliable enhancement and segmentation of capillaries in NC images is crucial to be able to extract morphological features and hence allow for accurate diagnosis. In this paper, we investigate the performance of five image enhancement techniques when integrated into three capillary skeleton extraction algorithms and evaluate their suitability with respect to the resulting skeletonisation performance.

2. Image Enhancement Techniques

In general, any kind of capillaroscopic image analysis starts with an image enhancement process. The choice of enhancement technique has a direct impact on the final result, since the image quality greatly influences the subsequent analysis. However in the literature, with the exception of[13,14], relatively little attention has been given to this preprocessing step.

In the following, we briefly discuss the five enhancement techniques that we evaluated in our study (for further details we refer to the original papers):

- *α-trimmed filter*[15]*:* a non-linear window-based filter. It can be considered as a hybrid filter derived from mean and median filters. If the pixel values x_k within a window around location (i, j) are sorted in ascending order $x_1 \leq x_2 \leq \cdots \leq x_N$, then the output of the α-trimmed filter is defined as

$$\hat{x}_{ij} = \frac{1}{N(1-\alpha_1-\alpha_2)} \sum_{k=\alpha_1 N+1}^{N-\alpha_2 N} x_k, \quad 0 \leq \alpha_1, \alpha_2 \leq 0.5, \tag{1}$$

  where α_1 and α_2 are the parameters of the filter.

- *Bilateral filter*[16]*:* a non-iterative, relatively simple algorithm which smoothens an image while preserving edges by means of a non-linear combination of nearby image values based on both their spatial closeness $c(\xi, x)$ and their photometric similarity $s(f(\xi), f(x))$. It is suggested that the two pixels can be close to one another (that is, occupy nearby spatial locations $c(\xi, x)$) or they can be similar to one another (that is, have nearby values $s(f(\xi), f(x))$). Bilateral filtering, basically the combination of domain and range filtering, is defined as

$$h(x) = \frac{\int_{\Omega(x)} f(\xi) c(\xi, x) s(f(\xi), f(x)) d\xi}{\int_{\Omega(x)} c(\xi, x) s(f(\xi), f(x)) d\xi}. \tag{2}$$

- *Bilateral enhancer*[17]*:* extends the concept of bilateral filters so that edge preserving smoothing and selective sharpening is performed simultaneously. A weighted average is utilised that is independent of the design of $c(.)$ and $s(.)$ in Eq. (2). Furthermore, it considers a special case when $\xi = x$ and adds a constant g in this case. This does not change the nature of the filter, but for $\xi = x$, the contribution of $c(.)$ and $s(.)$ is summarised into g. The bilateral enhancer is defined as

$$j(x) = g f(x) + \int_{\frac{\Omega(x)}{x}} c(\xi, x) p(f(x), f(\xi)) d\xi, \tag{3}$$

  where $g = c(x, x)s(f(x), f(x))$.

- *Anisotropic diffusion filtering*[18]*:* an iterative algorithm which smoothens an image using a diffusion function. Smoothing is formulated as a diffusive process which is stopped at boundaries by selecting locally adaptive diffusion strengths. Diffusion functions allow the diffusion process to take place in the interior of regions while not affecting edges. The anisotropic diffusion equation is defined as

$$I_t = div(c(\bar{x}, t)\nabla u(\bar{x}, t)), \tag{4}$$

where diffusion is controlled by varying $c(\bar{x}, t)$, and $u(\bar{x}, t)$ represents the image intensity. The resulting image is obtained after optimising $c(\bar{x}, t)$.

- *Non-local means (NLM)*[19]*:* a non-iterative algorithm which smoothens an image by a non-local averaging of all pixels in the image. The weights depend on the similarity between two pixels which are defined by the similarity of the intensity grey level in a square neighbourhood of fixed size. The similarity is measured as a decreasing function of weighted Euclidean distance. The NLM filter is defined as

$$NLM[v](i) = \sum_{j \in I} w(i, j)v(j), \tag{5}$$

where the weights $w(i, j)$ depend on the similarity between pixels i and j.

3. Nailfold capillary skeletonisation algorithms

In the following, we discuss the three NC skeletonisation algorithms that we employ in this study.

3.1. Wen et al.[9,10]

Wen *et al.*[9,10] first reduce the brightness of the image, and then perform histogram equalisation. A thresholding method is subsequently applied to arrive at a binarised image. The authors present an iterative skeletonisation algorithm where in each iteration every image pixel is checked against the following conditions:

- $2 \leq N(P_1) \leq 6$,
- $S(P_1) = 1$,
- $P_2 \times P_4 \times P_6 = 0$,
- $P_4 \times P_6 \times P_8 = 0$,

where $P_1 ... P_9$ are the nine pixels in a 3×3 window, $N(P_1)$ denotes the number of non-zero neighbours of P_1, and $S(P_1)$ is the number of zero to one changes from P_n to P_{n+1} with $1 < n < 9$.

If all conditions are met, the pixel is flagged. Flagged pixels are then assigned to the background. In a second step, pixels are inspected with regards to a second set of conditions, namely:

- $2 \leq N(P_1) \leq 6$,
- $S(P_1) = 1$,
- $P_2 \times P_4 \times P_8 = 0$,
- $P_2 \times P_6 \times P_8 = 0$.

Again, if all conditions are met, the pixel is flagged, and flagged pixels are removed from the image. This procedure is repeated until convergence, i.e., until no more pixels get flagged during an iteration. The resulting image then defines the capillary skeletons.

3.2. Lo et al.[20]

Lo *et al.* observe that the red and blue channels of NC images tend to be noisy while the green plane usually shows the highest degree of contrast to separate capillaries from the background and is consequently used for subsequent analysis. This channel is processed by local and global histogram equalisation methods in order to further enhance the contrast between background and capillaries. Otsu's thresholding method[21] is then used on both globally equalised and locally equalised images to produce a binary image where capillary areas are labelled with 0s and the background with 1s. Oversegmentation and image noise is reduced by applying global and local thresholding methods. Globally

thresholded images preserve the major non-capillary area while local thresholding allows for precise segmentation of capillaries. These images are then combined through a logical OR operation.

Since devised for NC video sequences, a number of frames are processed using the above algorithm and combined to generate one resulting binary image R. In our implementation, we slightly modify this step so as to work on static images rather than video sequences. In particular, we apply different block sizes for local thresholding and then all images are combined by

$$R(x,y) = \begin{cases} 0 & \text{if } count(x,y) \geq \zeta \\ 1 & \text{if } count(x,y) < \zeta \end{cases} \tag{6}$$

with

$$count(x,y) = \sum_{t=1}^{N} C(x,y,t), \tag{7}$$

and

$$C(x,y,t) = \begin{cases} 0 & \text{if } I(x,y,t) = 1 \\ 1 & \text{if } I(x,y,t) = 0 \end{cases} \tag{8}$$

where $t = 1 \ldots 10$ representing 10 block sizes changing from 5×5 to 50×50 in steps of 5, ζ is a threshold and $I(x,y,t)$ are the pixels of the image at position (x,y) locally thresholded within a block size of t.

Finally, a morphological (erosion-based) algorithm is iteratively applied to thin the capillaries and extract their skeletons.

3.3. Doshi et al.[22]

Doshi *et al.* employ a bilateral enhancer[17] for noise reduction, which is followed by histogram equalisation to improve the contrast in the image. NC images typically exhibit a fairly high degree of non-uniform illumination which makes them difficult to segment accurately. Capillary patterns have relatively high spatial frequencies, while varying illumination is characterised by low spatial frequencies. This issue is address by employing a difference of Gaussian (DoG) approach which effectively works as a band pass filter and is defined as

$$h(x,y) = \frac{1}{2\pi}\left[\frac{1}{\sigma_1^2} exp\left(-\frac{x^2+y^2}{2\sigma_1^2}\right) - \frac{1}{\sigma_2^2} exp\left(-\frac{x^2+y^2}{2\sigma_2^2}\right)\right], \tag{9}$$

where $\sigma_1 < \sigma_2$, σ_2 is set as the average capillary radius and $\sigma_2/\sigma_1 = 1.6$. In our implementation, we set $\sigma_2 = 4$ and the block size of the Gaussian filter to 18.

After image enhancement, a binarisation step is conducted to arrive at a representation where capillaries are separated from the background. This is achieved through thresholding using Otsu's algorithm[21], which is then followed by two iterations of a median filter to remove small and isolated objects.

The skeletons of the capillaries are extracted using a thinning algorithm based on[23]. Here, based on 8-pixel connectivity to preserve curvature information, the following conditions are iteratively checked for each pixel:

- $C(P) = 1$,
- $2 \leq N(P) \leq 3$,
- One of the following
  - $(P_2 \vee P_3 \vee P_5) \vee P_4 = 0$ in odd iterations,
  - $(P_6 \vee P_7 \vee P_1) \wedge P_8 = 0$ in even iterations,

where P_2, P_4, P_6 and P_8 are the immediate neighbours and P_1, P_3, P_5 and P_7 the diagonal neighbours of the inspected pixel P, $C(P)$ denotes the number of distinct 8-connected components of 1s in the pixel's neighbourhood, with $N(P) = \min(N_1(P), N_2(P))$, $N_1(P) = (P_1 \vee P_2) + (P_3 \vee P_4) + (P_5 \vee P_6) + (P_7 \vee P_8)$, and $N_2(P) = (P_2 \vee P_3) + (P_4 \vee P_5) + (P_6 \vee P_7) + (P_8 \vee P_1)$, where $\vee$ represents a logical OR and $\wedge$ a logical AND. Pixels which satisfy these conditions are assigned to the background and the next iteration is started to check the same set of conditions. The process terminates when no more pixels are removed; the resulting image then defines the capillary skeletons.

4. Experimental Evaluation

In our experiments, we embedded the five enhancement techniques discussed in Section 2 in the three skeletonisation algorithms explained in Section 3 and inspect the resulting skeletonisation performance, both in terms of visual results as a quantitative analysis.

For evaluation, we used a set of NC images obtained at the Dermatology Unit, Clinical Hospital of Chieti using an Olympus SZ40 stereo microscope coupled with an external light source. To arrive at a set of representative images, we chose two NC images of each of the following groups: *control*, *early*, *active*, and *late* which correspond to typical classes of NC based diagnosis[6].

The various parameters for the enhancement algorithms were set (empirically) as follows. For the α-trimmed filter, we chose $\alpha_1 = \alpha_2 = 0.5$. For anisotropic diffusion, we used 15 iterations and an integration constant of 0.14; κ which controls diffusion was set to 30. For the bilateral filter, a Gaussian of size 3 and with $\sigma = 0.1$ was chosen, while the smoothing and enhancement factors in the bilateral enhancer were set to 0.3, with $g = 1$, $n_e = 0.5$, and $n_s = 1$. NLM filtering was implemented with a radio search window of 5, a radio similarity window of 2 and a degree of filtering of 8.

For quantitative performance evaluation, in each image a region of interest (containing capillaries) is considered and manually defined ground truth skeletons obtained for that region. As performance measure we employ Pratt's figure of merit[24] which is a well-known measure to express the closeness of a generated edge map to an ideal (ground truth) edge map, where a higher figure of merit signifies better agreement with the ground truth. If I_I and I_A are the number of ideal and actual skeleton points, $d(i)$ the pixel missed distance of the i-th skeleton point detected, and α a scaling constant, then the figure of merit (FoM) is defined as

$$\text{FoM} = \frac{1}{\max\{I_I, I_A\}} \sum_{i=1}^{I_A} \frac{1}{1 + \alpha d^2(i)}, \tag{10}$$

and penalises missing valid skeleton points, displaced skeleton points and classification of noise as skeleton points.

Baseline results, for all images and the three original skeletonisation algorithms, are given in Table 1. From there, it is evident that the approach by Doshi *et al.* outperforms both other algorithms, giving an average figure of merit of 0.35 which is clearly superior to the 0.20 achieved by Wen *et al.* and the 0.10 by Lo *et al.*. The main reason for this is that Doshi *et al.*'s algorithm better accounts for illumination and brightness variance within the image, which in turn leads to improved binarisation results. We can also see that there is clearly scope for improvement, considering that perfect skeletonisation would yield a FoM of 1.0. In particular, the results on the *late* images are quite poor for all three methods, since these were both of poorer image quality compared to the others and as the capillary structures in there are of higher complexity.

Table 2 gives the results of integrating the various image enhancement techniques into the skeletonisation algorithms. For the methods by Wen *et al.* and Lo *et al.* this means applying the various image denoising/enhancement methods prior to the actual algorithms. For Doshi *et al.*'s algorithm, the bilateral enhancer is replaced with the other

Table 1. Baseline results for the three skeletonisation algorithms.

	Wen *et al.*[10]	Lo *et al.*[20]	Doshi *et al.*[22]
Control 1	0.33	0.09	0.45
Control 2	0.10	0.10	0.40
Early 1	0.26	0.12	0.48
Early 2	0.10	0.04	0.12
Active 1	0.16	0.21	0.45
Active 2	0.20	0.06	0.29
Late 1	0.12	0.05	0.14
Late 2	0.10	0.04	0.15
average	0.20	0.10	0.35

Table 2. Results for combining image enhancement techniques and skeletonisation algorithms.

	α-trimmed filter			Bilateral filter			Bilateral enhancer			Anisotropic diffusion			Non-local means		
	Wen	Lo	Doshi	Wen	Lo	Doshi	Wen	Lo	Doshi	Wen	Lo	Doshi	Wen	Lo	Doshi
Control 1	0.56	0.08	0.44	0.29	0.14	0.43	0.34	0.11	0.45	0.20	0.10	0.41	0.29	0.15	0.43
Control 2	0.21	0.10	0.43	0.28	0.20	0.34	0.38	0.19	0.34	0.28	0.12	0.22	0.46	0.19	0.30
Early 1	0.35	0.18	0.52	0.27	0.25	0.37	0.25	0.23	0.39	0.27	0.16	0.36	0.21	0.25	0.36
Early 2	0.18	0.06	0.13	0.16	0.11	0.15	0.23	0.09	0.15	0.20	0.11	0.13	0.24	0.10	0.12
Active 1	0.36	0.21	0.61	0.11	0.36	0.61	0.29	0.27	0.62	0.04	0.24	0.59	0.33	0.40	0.64
Active 2	0.51	0.09	0.41	0.00	0.17	0.41	0.16	0.11	0.42	0.00	0.10	0.37	0.00	0.16	0.47
Late 1	0.18	0.07	0.21	0.23	0.07	0.17	0.15	0.04	0.16	0.09	0.04	0.17	0.13	0.05	0.11
Late 2	0.29	0.06	0.39	0.14	0.08	0.33	0.20	0.07	0.36	0.09	0.07	0.27	0.26	0.08	0.27
average	0.38	0.12	0.45	0.21	0.19	0.40	0.29	0.16	0.41	0.17	0.14	0.36	0.27	0.20	0.39

enhancement methods. We also found the histogram equalisation step of Doshi *et al.*'s to be unnecessary and actually to lead to lower performance and hence discarded it. For Wen *et al.* method, since no threshold is specified in the algorithm, we run the experiments for multiple thresholds ranging from 10 to 250 and selecting the best value over all images.

From Table 2, it is clear that modifying the pre-processing step of the various algorithms can improve the resulting skeletonisation accuracy. The algorithms of Doshi *et al.* and Lo *et al.* are improved by almost 10%, whereas the performance of Wen *et al.*'s algorithm is improved by 18%.

Interestingly, the α-trimmed filter, albeit being the simplest of the investigated approaches, leads to the highest accuracy for Wen *et al.*'s and Doshi *et al.*'s algorithms. For Lo *et al.*'s approach, non-local means filtering leads to the best performance. The bilateral enhancer leads to the second best performance for Wen *et al.*'s and Doshi *et al.*'s algorithms, while the bilateral filter gives the second best results for Lo *et al.*'s method. The results also show that the omission of the histogram equalisation step for Doshi et al.'s algorithm leads to better skeletonisation accuracy.

Comparing the results from Table 1 with those from Table 2 results, we can see that all enhancement techniques lead to improved performance for all algorithms except for Wen *et al.* using anisotropic diffusion filtering. The α-trimmed filter gives an improvement of 30%, bilateral enhancer and NLM filtering of 21%, and the bilateral filter of 15%; the lowest performance improvement is observed for anisotropic diffusion (5%). ethods have shown bias towards one particular method.

Now looking at Fig. 1, which shows some visual results for *control* and *early* images, we can observe that the skeleton images using α-trimmed filter (h,m,r) are nosier than the other images. The best performance using Doshi *et al.*'s method is due to obtaining a uniform background using a DoG filter. The other filters (d,e,f,g) lead to comparatively less noise in the image, but often at the expense of missing out completely some of the capillaries.

Turning our attention the Fig. 2, where *active* and *late* group images are shown, the same effect is observed. It clear that Doshi *et al.*'s method to binarised the image works well in tandem with the enhancement techniques and is capable of tackling most of the noise in the images. However, for the *late* image in Figure 2, the image quality is rather poor and consequently it is difficult to extract the capillary skeletons.

Overall, an α-trimmed filter along with Doshi *et al.*'s method gives the best performance, while Lo *et al.*'s algorithm together with α-trimmed filter leads to the worst skeletonisation accuracy. The stark difference between the obtained results confirms that choosing an appropriate image enhancement technique is indeed crucial and also that this choice depends on the subsequent processing stages.

5. Conclusions

Nailfold capillaroscopy (NC) is a passive, inexpensive in-vivo technique to observe micro-blood vessel characteristics in the nailfold region of fingers. NC is of particular importance in diagnosing diseases that lead to morphological changes of capillaries such as scleroderma, Raynaud's phenomenon and other connective tissue diseases. Inspection of NC images is typically performed manually and thus constitutes a time consuming and specialised task which motivates the use of a computer-aided diagnosis (CAD) approach. Such CAD systems however depend on reliable enhancement of the capillaries structures in the images. In this paper, we have evaluated five image enhancement tech-

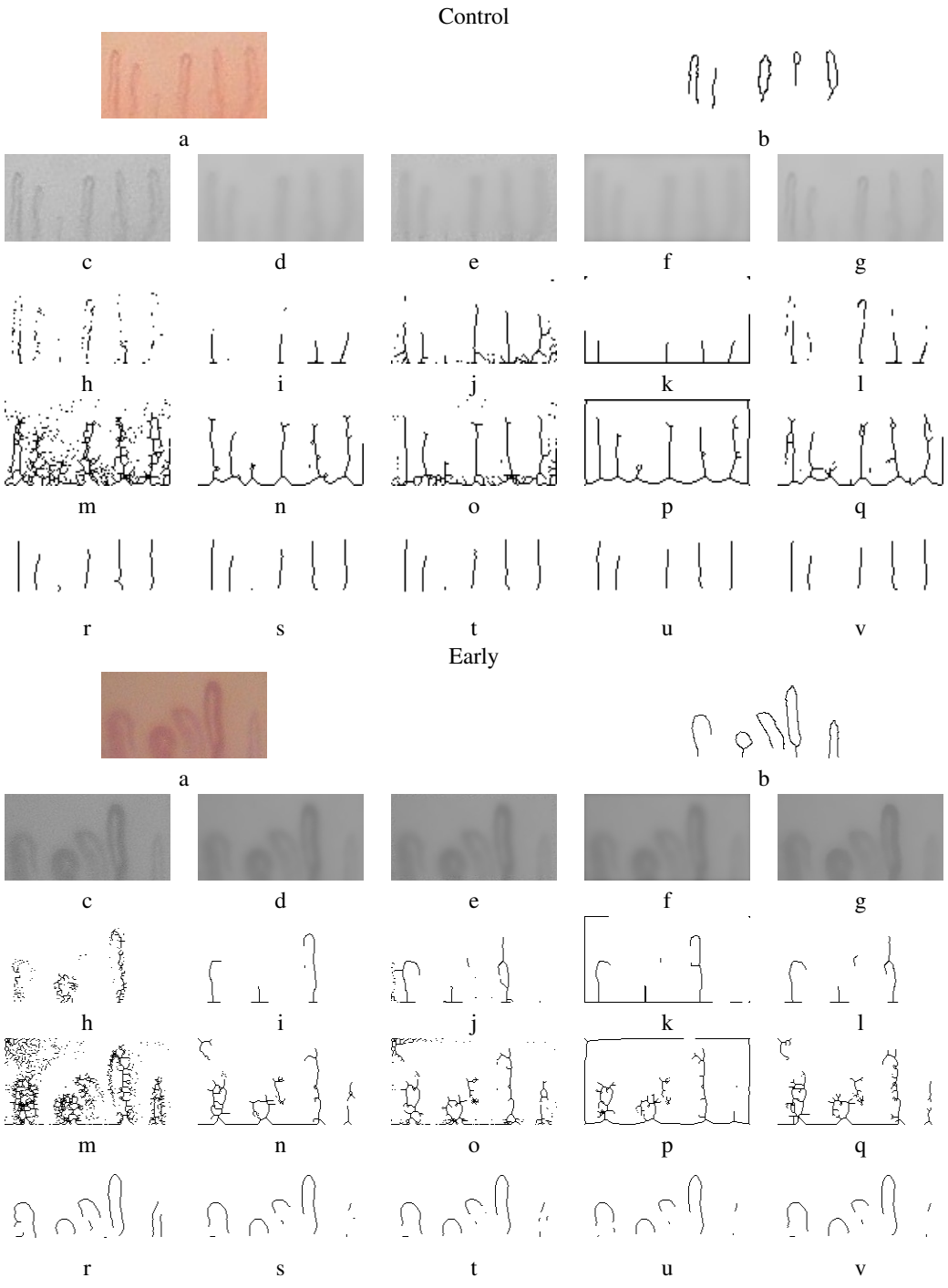

Fig. 1. Example NC images and their results: *control* (top) and *early* pattern (bottom). For each image we show: (a) the ROI image; (b) the groundtruth image skeleton of image in (a); (c)-(g) after pre-processing using α-trimmed filter, bilateral filter, bilateral enhancer, anisotropic diffusion filter and non-local means; (h)-(l) after skeletonisation using Wen *et al.*'s algorithm for all images in (c)-(g); (m)-(q) after skeletonisation using Lo *et al.*'s algorithm for all images in (c)-(g); (r)-(v) after skeletonisation using Doshi *et al.*'s algorithm for all images in (c)-(g). All processed images were inverted for display purposes.

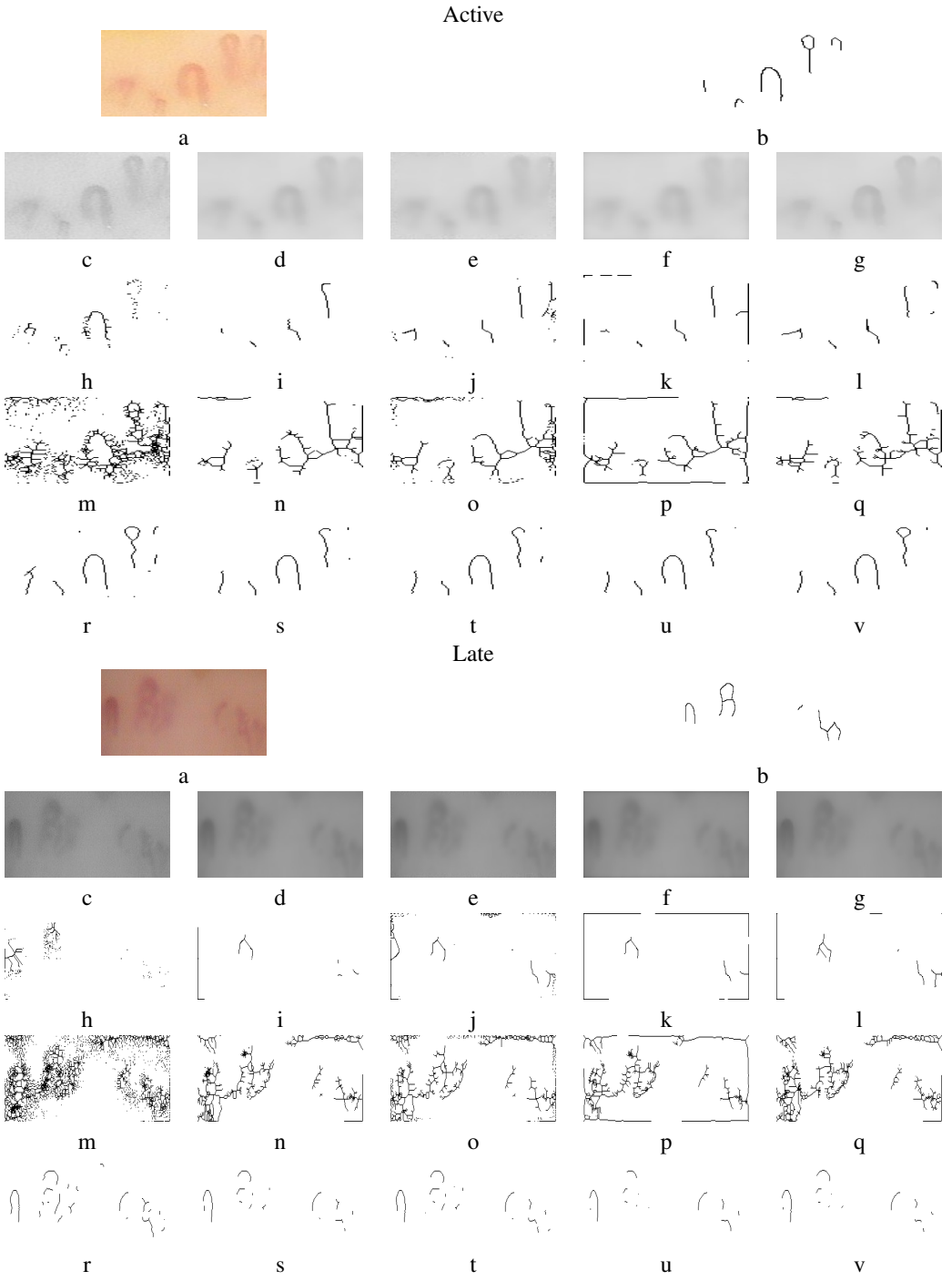

Fig. 2. Example NC images and their results: *active* (top) and *late* pattern (bottom), arranged in the same layout as Figure 1.

niques in combination with three capillary skeletonisation algorithms on a challenging dataset of NC images. Both visual inspection and quantitative evaluation based a manually defined ground truth show that α-trimmed filter along with a skeletonisation algorithm incorporating a difference-of-Gaussian approach to address non-uniform lighting and an iterative rule-based skeletonisation procedure leads to the best overall performance.

References

1. Grassi, W., Medico, P.D., Izzo, F., Cervini, C.. Microvascular involvement in systemic sclerosis: Capillaroscopic findings. *Seminars in Arthritis and Rheumatism* 2001;**30**(6):397–402.
2. Cutolo, M., Grassi, W., Matucci Cerinic, M.. Raynaud's phenomenon and the role of capillaroscopy. *Arthritis & Rheumatism* 2003; **48**(11):3023–3030.
3. Cutolo, M., Sulli, A., Secchi, M., Paolino, S., Pizzorni, C.. Nailfold capillaroscopy is useful for the diagnosis and follow-up of autoimmune rheumatic diseases. a future tool for the analysis of micro-vascular heart involvement? *Rheumatology* 2006;**45 Suppl 4**(ii):iv43–iv46.
4. Tektonidou, M., Kaskani, E., Skopouli, F.N., Moutsopoulos, H.M.. Microvascular abnormalities in Sjgren's syndrome: nailfold capillaroscopy. *Rheumatology* 1999;**38**(9):826–830.
5. Cutolo, M., Pizzorni, C., Sulli, A.. Capillaroscopy. *Best Practice and Research Clinical Rheumatology* 2005;**19**(3):437–452.
6. Cutolo, M., Sulli, A., Pizzorni, C., Accardo, S.. Nailfold videocapillaroscopy assessment of microvascular damage in systemic sclerosis. *The Journal of Rheumatology* 2000;**27**:155–60.
7. Allen, P.D., Taylor, C.J., Herrick, A.L., Moore, T.. Image analysis of nailfold capillary patterns from video sequences. In: *Medical Image Computing and Computer-Assisted Intervention*; vol. 1679 of *Lecture Notes in Computer Science*. 1999, p. 698–705.
8. Paradowski, M., Markowska-Kaczmar, U., Kwasnicka, H., Borysewicz, K.. Capillary abnormalities detection using vessel thickness and curvature analysis. In: *13th Int. Conference on Knowledge-Based and Intelligent Information and Engineering Systems*. 2009, p. 151–158.
9. Wen, C.H., Liao, W.D., Li, K.C.. Classification framework for nailfold capillary microscopy images. In: *10th IEEE Region Conference TENCON*. 2007, p. 1–4.
10. Wen, C.H., Hsieh, T.Y., Liao, W.D., Lan, J.L., Chen, D.Y., Li, K.C., et al. A novel method for classification of high-resolution nailfold capillary microscopy images. In: *1st IEEE International Conference on Ubi-Media Computing*. 2008, p. 513–518.
11. Wen, C.H., Liao, W.D., Hsieh, T.Y., Chen, D.Y., Lan, J.L., Li, K.C.. Computer-aided image analysis aids early diagnosis of connective-tissue diseases. In: *SPIE Newsroom, Biomedical Optics & Medical Imaging*. 2009, .
12. Doshi, N.P., Schaefer, G., Merla, A.. Nailfold capillaroscopy pattern recognition using texture analysis. In: *IEEE-EMBS Int. Conference on Biomedical and Health Informatics*. 2012, .
13. Doshi, N.P., Schaefer, G., Merla, A.. Enhancement of nailfold capillaroscopy images. In: *IEEE-EMBS Int. Conference on Biomedical and Health Informatics*. 2012, .
14. Doshi, N.P., Schaefer, G., Merla, A.. An evaluation of image enhancement techniques for capillary imaging. In: *IEEE Int. Conference on Systems, Man, and Cybernetics*. 2012, .
15. Zhong, J., Asker, C.L., Salerud, E.G.. Imaging, image processing and pattern analysis of skin capillary ensembles. *Skin Research and Technology* 2000;**6**(2):45–57.
16. Tomasi, C., Manduchi, R.. Bilateral filtering for gray and color images. In: *6th Int. Conference on Computer Vision*. 1998, p. 839–846.
17. Gatta, C., Radeva, P.. Bilateral enhancers. In: *16th IEEE International Conference on Image Processing*. 2009, p. 3161–3164.
18. Perona, P., Malik, J.. Scale-space and edge detection using anisotropic diffusion. *IEEE Transactions on Pattern Analysis and Machine Intelligence* 1990;**12**(7):629 –639.
19. Buades, A., Coll, B., Morel, J.M.. A non-local algorithm for image denoising. In: *IEEE Computer Society Conference on Computer Vision and Pattern Recognition*; vol. 2. 2005, p. 60 – 65 vol. 2.
20. Lo, L.C., Chiang, J., Cai, Y.S.. Three-dimensional vision-based nail-fold morphological and hemodynamic analysis. In: *11th IEEE International Conference on Bioinformatics and Bioengineering*. 2011, p. 44 –51.
21. Otsu, N.. A threshold selection method from gray-level histograms. *IEEE Transactions on Systems, Man and Cybernetics,* 1979;**9**(1):62 –66.
22. Doshi, N.P., Schaefer, G., Merla, A.. Robust nailfold capillary skeleton extraction. In: *5th Int. Conference on Emerging Trends in Engineering and Technology*. 2012, p. 19–23.
23. Guo, Z., Hall, R.W.. Parallel thinning with two-subiteration algorithms. *Commun ACM* 1989;**32**(3):359–373.
24. Abdou, I., Pratt, W.. Quantitative design and evaluation of enhancement/thresholding edge detectors. *Proceedings of the IEEE* 1979; **67**(5):753–763.